




NICLOSAMIDE-EXFOLIATED ANIONIC CLAY NANOHYBRID REPURPOSED AS AN ANTIVIRAL DRUG FOR TACKLING COVID-19; ORAL FORMULATION WITH TWEEN 60/EUDRAGIT S100

N. SANOJ REJINOLD¹, HUIYAN PIAO¹, GOEUN CHOI^{1,2,3}, GEUN-WOO JIN⁴, AND
JIN-HO CHOY^{1,5,6*} 

¹Intelligent Nanohybrid Materials Laboratory (INML), Institute of Tissue Regeneration Engineering (ITREN), Dankook University, Cheonan 31116, Korea

²College of Science and Technology, Dankook University, Cheonan 31116, Korea

³Department of Nanobiomedical Science and BK21 PLUS NBM Global Research Centre for Regenerative Medicine, Dankook University, Cheonan 31116, Korea

⁴R&D Centre, CnPharm Co., LTD., Seoul 03759, Korea

⁵Department of Pre-medical Course, College of Medicine, Dankook University, Cheonan 31116, Korea

⁶Tokyo Tech World Research Hub Initiative (WRHI), Institute of Innovative Research, Tokyo Institute of Technology, Yokohama 226-8503, Japan

Abstract—The ongoing pandemic, COVID-19 (SARS-CoV-2), has afflicted millions of people around the world, necessitating that the scientific community work, diligently and promptly, on suitable medicaments. Although vaccination programs have been run globally, the new variants of COVID-19 make it difficult to restrict the spread of the virus by vaccination alone. The combination of vaccination with anti-viral drug formulation is an ideal strategy for tackling the current pandemic situation. Drugs approved by the United States Food and Drug Administration (FDA), such as Remdesivir, have been found to be of little or no benefit. On the other hand, re-purposing of FDA-approved drugs, such as niclosamide (NIC), has offered promise but its applicability is limited due to its poor aqueous solubility and, therefore, low bioavailability. With advanced nano-pharmaceutical approaches, re-purposing this drug in a suitable drug-carrier for a better outcome may be possible. In the current study, an attempt was made to explore the loading of NIC into exfoliated layered double hydroxide nanoparticles (X-LDH NPs); prepared NIC-X-LDH NPs were further modified with eudragit S100 (ES100), an enteric coating polymer, to make the final product, ES100-NIC-X-LDH NPs, to improve absorption by the gastro/intestinal tract (GIT). Furthermore, Tween 60 was added as a coating on ES100-NIC-X-LDH NPs, not just to enhance its in vitro and in vivo stability, but also to enhance its mucoadhesive property, and to obtain, ultimately, better in vivo pharmacokinetic (PK) parameters upon oral administration. Release of NIC from Tween 60-ES100-NIC-X-LDH NPs was found to be greater under gastro/intestinal solution within a shorter period of time than the uncoated samples. The in vivo analysis revealed that Tween 60-ES100-NIC-X-LDH NPs were able to maintain a therapeutically relevant NIC plasma concentration in terms of PK parameters compared to the commercially available Yomesan®, proving that the new formulation might prove to be an effective oral drug-delivery system to deal with the SARS-CoV-2 viral infections. Further studies are required to ensure their safety and anti-viral efficacy.

Keywords—COVID-19 · Exfoliated layered double hydroxide nanoparticles · Niclosamide · Oral formulation · Pharmacokinetics

INTRODUCTION

COVID-19 has affected ~199 M individuals, resulting in ~4.24 M deaths worldwide as of August 3, 2021. The scientific community has made tireless efforts to find a suitable remedy for COVID-19 since it was first reported in China's Wuhan Province (Yamamoto et al., 2020; Li et al., 2021; Mei et al., 2021; Yang et al., 2021; Zhu et al., 2021). Of most concern at present is the arrival of new, mutated, genetic variants (e.g. the delta variant), suspected to be much more contagious than the original SARS-CoV-2 virus (Hu et al., 2020). Clearly, vaccination alone cannot restrict the viral spread; much uncertainty exists about the longevity of immunity acquired from various vaccinations. An urgent need exists, therefore, for scientists to

come up with novel formulation(s) that could be used in the fight against the COVID-19.

Several FDA-approved drugs could be useful if re-purposed for treatment against COVID-19 (Jeon et al., 2020). A recent study reported that almost 24 drug candidates were suggested as potential anti-viral drugs in the fight against COVID-19 (Jeon et al., 2020). Most have half-maximal inhibitory concentration (IC₅₀) values ranging from 0.1 to ~10 μM. Among them, niclosamide (NIC) showed significantly greater therapeutic efficacy, having an IC₅₀ of 0.28 μM against SARS-CoV-2, better than many other drugs, such as cyclosporin, imodium, lariam, amdaquine, proscillaridin, digitaline, lanoxin, nabac, salinomycin, ouabain, cepharanthine, ciclesonide, oxyclozanide, anidulafungin, gilteritinib, berbamine, tetrandrine, abemaciclib, ivacaftor, bazedoxifene, and eltrombopag (Jeon et al., 2020).

NIC is an FDA-approved anthelmintic drug, which has been used previously in anti-parasitic (Kao et al., 2018), anti-inflammatory (Huang et al., 2015), and anti-cancer

* E-mail address of corresponding author: jhchoy@dankook.ac.kr
DOI: 10.1007/s42860-021-00153-6

(Yu et al., 2018) drug formulations. NIC has limited application, however, because of its poor solubility, and, as a consequence, very low bio-availability (Grifasi et al., 2015). Various approaches have been made to improve its solubility through chemical modification (Ma et al., 2020), nano-encapsulation (Hatamipour et al., 2019), and co-crystallization, etc. (Grifasi et al., 2015). For example, polyethyleneglycol (PEG) was modified with NIC to improve its solubility and, thereby, its effective therapeutic benefits in relation to CT26 (Mouse colon carcinoma cells). Such experimental results clearly paved the way for proving that suitably modified NIC formulations could serve as potential drugs for treating viral diseases such as COVID-19.

Most of the NIC-modified formulations were related to cancer therapy; the present pandemic situation requires an alternative medicinal formulation for a quick solution. In this context, loading NIC in a desirable drug carrier is important. Among the various drug carriers that have been tried, inorganic materials such as exfoliated layered double hydroxides (X-LDH) play a vital role because of their excellent biocompatibility and biodegradability (Choi, 2018b; Choi et al., 2021b; Choi & Choy, 2021). LDH-based hybrid NPs have been used widely, therefore, particularly for drug delivery (Yan et al., 2019), bio-imaging (Jin & Park, 2019), and tissue engineering (Belgheisi et al., 2020).

The purpose of the current study was to hybridize the biocompatible X-LDH NPs with NIC to form NIC-X-LDH NPs, and thereafter to functionalize the NIC-X-LDH NPs with eudragit S100 (ES100), as an enteric coating agent, to make it responsive at precisely the intestinal pH of 6.8. In order to stabilize and induce fast drug release, Tween 60 was also added as a coating on ES100-NIC-X-LDH NPs for the final oral formulation, which is referred to below as Tween 60-ES100-NIC-X-LDH NPs (Fig. 1).

The major research questions addressed here were: (1) How effectively can the as-made oral formulation act as an NIC-delivery agent? (2) What would be the in vivo PK profile for NIC from the orally administered formulation?

(i) The proposal here is that Tween 60-ES100-NIC-X-LDH-NPs would allow effective NIC delivery because of their various functional properties where X-LDH NPs would enhance a clathrin-mediated endocytosis, while pH-sensitive drug release can be achieved from the ES100 component. The Tween 60 would enhance both stability as well as solubility of NIC from Tween 60-ES100-NIC-X-LDH NPs. (ii) When administered orally, the NIC nanohybrid NPs (Tween 60-ES100-NIC-X-LDH NPs) being muco-adhesive, can be retained for longer in the gastrointestinal tract (GIT) and thereby facilitate sustained release of NIC, resulting in an improved bioavailability.

MATERIALS AND METHODS

Materials

NIC ($C_{13}H_8C_{12}N_2O_4$) was purchased from Derivados Quimicos, Murcia, Spain. Anhydrous Ethanol (99.9%) and

isopropyl alcohol (IPA) were purchased from Daejung, Gyeonggi-do, South Korea. Magnesium nitrate hexahydrate [$Mg(NO_3)_2 \cdot 6H_2O$], aluminum nitrate nonahydrate [$Al(NO_3)_3 \cdot 9H_2O$], sodium hydroxide (NaOH), and formamide (CH_3NO) were obtained from Daejung Co. Ltd., Gyeonggi-do, South Korea. ES100 was purchased from EVONIK (Darmstadt, Germany) and Tween 60 was purchased from TCI (Tokyo, Japan).

Synthesis of Exfoliated Layered Double Hydroxide Nanoparticles (X-LDH NPs)

A co-precipitation method was used to make pristine LDH (Choi et al., 2018a). Initially, a solution mixture of $Mg(NO_3)_2 \cdot 6H_2O$ (0.012 M) and $Al(NO_3)_3 \cdot 9H_2O$ (0.006 M) was titrated with 0.5 M NaOH solution. The pH of the solution was adjusted to 10.5 ± 0.2 . The subsequent white precipitate was then kept for a 3 h aging process in an N_2 atmosphere, and further kept in a $100^\circ C$ hydrothermal process for one day. Decarbonated water was used to wash the precipitate; then it was freeze-dried. In order to prepare the X-LDH NPs, initially pristine LDH was treated with formamide (0.2 g/100 mL) and kept for 3 days under mechanical stirring until it formed a stable colloidal solution. Then it was centrifuged at $2314 \times g$ for 5 min to separate the uniformly dispersed nanosheets of X-LDH from those sheets that had not been exfoliated, which were finally used for the experiments (Ma et al., 2006; Ansy et al., 2018). Because formamide is highly polar (polarity index: 7.3) due to its carbonyl group (C=O) at one end, a strong hydrogen bonding interaction could be expected with the -OH groups of X-LDH. As a result, the replacement of interlayer water with formamide disrupted the original interlayer attraction force allowing the exfoliation process (Ma et al., 2006).

Synthesis of Tween 60-ES100-NIC-X-LDH NPs

The detailed synthesis steps are illustrated in Fig. 2. In the initial step, 1 g of NIC was dissolved completely in 100 mL of anhydrous ethanol, which was then added to 100 mL of distilled water + X-LDH NPs dispersed in 75 mL of formamide (150 mg). Then, 200 mg of enteric coating agent ES100 (dissolved in 50 mL of ethanol) was coated on NIC-X-LDH NPs, and further centrifuged at $6429 \times g$ for 5 min in order to separate the loaded NIC from un-loaded, then freeze-dried for 2 days to obtain ES100-NIC-X-LDH NPs. Finally, Tween 60 was added as a coating by dispersing the ES100-NIC-X-LDH NPs in 99.9% ethanol for ~30 min, and then the solution obtained was dried under a rotary evaporator (Heidolph Instruments Gm bH & Co. KG, Schwabach, Germany) to obtain the dry powder for the oral formulation desired, Tween 60-ES100-NIC-X-LDH NPs, where the Tween 60 content was 40%.

Recrystallization of NIC under Various Solvents and Solute Conditions

Recrystallization experiments were carried out under various solvents and solute conditions in order to understand the crystalline nature of NIC under such conditions. Several

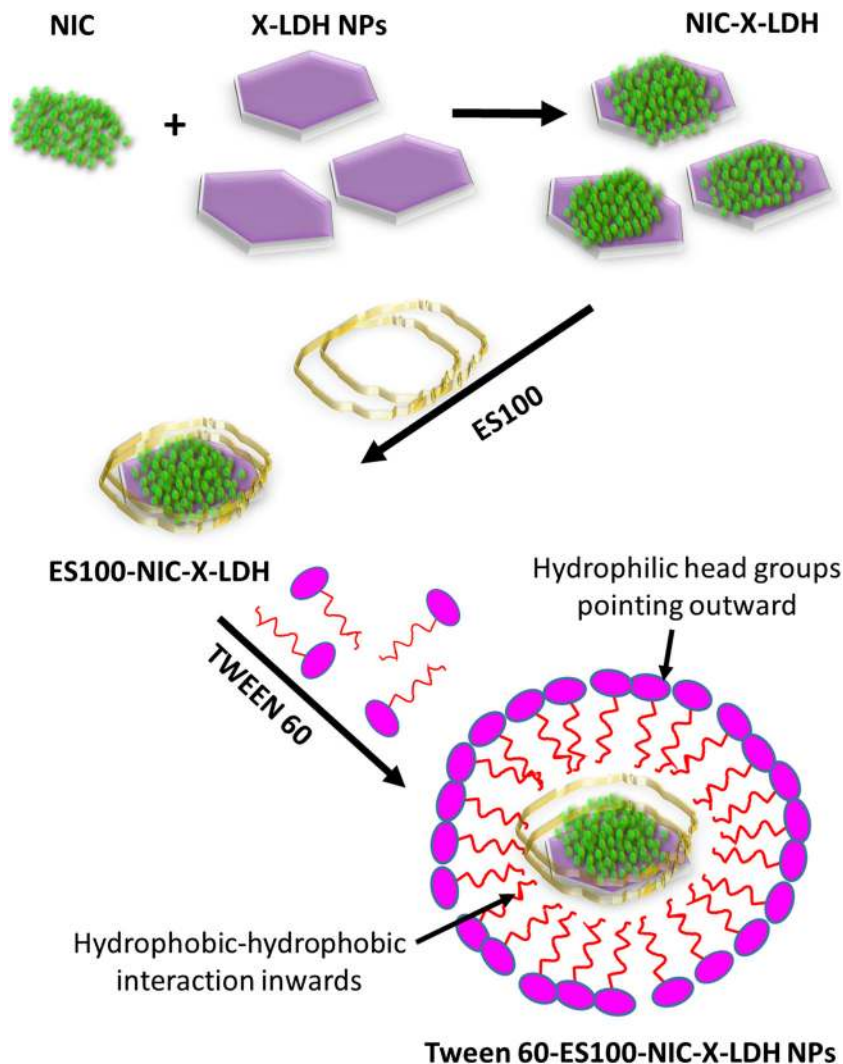


Fig. 1. The research strategy using Tween 60-ES100-NIC-X-LDH NPs. These NPs would enhance the NIC release based on the Tween 60 coating followed by a pH-sensitive swelling under intestinal pH, eventually improving the PK parameters. At first, NIC can be attached to the surface of X-LDH via active interaction through the $-OH$ functionalities present on the X-LDH surface. Secondly, the ES100 polymer could be attached on the X-LDH/NIC either physically or chemically through weak forces such as hydrogen bonding. Finally, Tween 60 coating was done mainly for imparting NIC solubility and stability for the Tween 60-ES100-NIC-X-LDH NPs

experiments were conducted as follows. All of the dried powders were analyzed by XRD.

Recrystallization of NIC in ethanol. For this, 1 g of NIC was dissolved in 100 mL of ethanol (99.9%) and stirred for ~15 min until dissolved completely. Thereafter, the solvent was evaporated using a rotary evaporator (Heidolph Instruments Gm bH & Co. KG, Schwabach, Germany) for ~15 min to obtain the dry powder.

Recrystallization of NIC in ethanol/distilled water. For this, 1 g of NIC was dissolved in 100 mL of ethanol (99.9%) and then stirred for ~15 min until dissolved completely. Thereafter, 100 mL of distilled water was added to the

solution above, forming a yellow/white precipitate which was then dried under a rotary evaporator for ~15 min to obtain the powder.

Recrystallization of NIC in formamide. 1 g of NIC was partially dissolved in 75 mL of formamide, which was then transferred to a 110 mm glass petri dish and heated to 60°C to achieve complete dissolution. Formamide was difficult to separate from the solution using rotary evaporation, as the boiling point is very high (~210°C). Once the NIC/formamide solution was dissolved at 60°C, it was cooled to RT (room temperature), allowing precipitation of NIC crystals that were collected after 12 h using 110 mm Whatman filter paper and then dried at 60°C for 3 h in a hot-air oven.

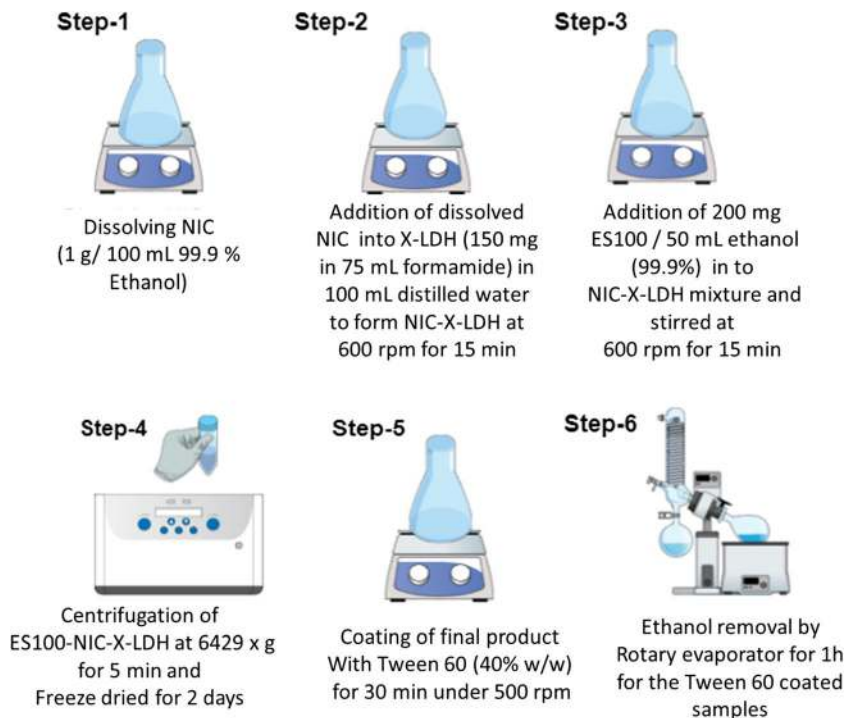


Fig. 2. Detailed synthesis for Tween 60-coated ES100-NIC-X-LDH NPs

Recrystallization of NIC in formamide/distilled water. 1 g of NIC was partially dissolved in 75 mL of formamide, then 100 mL of distilled water was added and the solution was stirred for 30 min. Once the NIC was dissolved at 60°C, it was cooled to RT, allowing precipitation of the NIC crystals, which then were collected (12 h) using 110 mm Whatman filter paper and dried in a hot-air oven at 60°C for 3 h.

Recrystallization of NIC in ethanol/formamide/distilled water. 1 g of NIC was dissolved fully in 100 mL of ethanol, to which 75 mL of formamide and 100 mL of distilled water were added. The whole solution was stirred for 60 min; the addition of formamide/distilled water resulted in partly dissolved NIC precipitates which were then dissolved at 60°C, and cooled to RT allowing precipitation of NIC crystals, which were collected (12 h) by Whatman filter paper and dried in a hot-air oven at 60°C for 3 h.

Recrystallization of NIC in ethanol/formamide. 1 g of NIC was dissolved fully in 100 mL of ethanol, to which was added 75 mL of formamide and the whole solution was stirred for 60 min. The addition of formamide resulted in only partially dissolved NIC precipitates, so the temperature was raised to 60°C, at which point complete dissolution occurred. The solution was then cooled to RT, which caused precipitation of NIC crystals that were collected by Whatman filter paper (12 h), and further dried in a hot-air oven at 60°C for 3 h.

Recrystallization of NIC in X-LDH NPs/formamide. 1 g of NIC was dissolved in 75 mL of formamide containing X-LDH

NPs (X-LD NPs ~150 mg), followed by continuous stirring for 15 min. The solubility of NIC in formamide/X-LDH NPs was only partial, so the temperature was raised to 60°C to effect complete dissolution. It was then cooled to RT to allow precipitation of the NIC crystals, and the resulting powder comprising NIC in X-LDH NPs was collected using Whatman filter paper (12 h) in a hot-air oven.

Recrystallization of NIC in X-LDH/formamide/Tween 60. Initially, 1 g of NIC was dissolved in 75 mL of formamide solution containing ~ 150 mg X-LDH NPs and stirred continuously for 15 min. 40% Tween 60 was mixed with the above solution and then the mixture was dissolved at 60°C, cooled to RT for precipitation of NIC crystals, and the solids were recovered as before, followed by drying (12 h) in a hot-air oven.

Recrystallization of NIC in ES100/ethanol. 1 g of NIC was dissolved in 100 mL of ethanol and 200 mg of ES100/50 mL ethanol was added to it. The whole solution was stirred for 15 min and the solvent was evaporated using a rotary evaporator for 10 min to obtain powdered samples.

Recrystallization of NIC in ES100/ethanol/Tween 60. 1 g of NIC was dissolved in 100 mL of ethanol and 200 mg of ES100, then a further 50 mL of ethanol was added to it, followed by 40% Tween 60 (~480 mg) and stirred for 15 min. The solvent was evaporated using a rotary evaporator for 10 min to obtain the powdered samples which were analyzed by XRD.

Recrystallization of NIC in ethanol/formamide/Tween 60. 1 g of NIC was initially dissolved in 100 mL of ethanol and then 75 mL of formamide was mixed with the solution and stirred for 30 min. Thereafter, 40% Tween 60 (~480 mg) was added. The solution was dissolved at 60°C, then cooled to RT, allowing precipitation of NIC crystals which were collected (12 h) in a hot air oven.

NIC Content Analysis

To measure the NIC content in the final formulations, samples of X-LDH-NIC, ES100-NIC-X-LDH NPs, and the Tween 60-coated solution were mixed thoroughly with 99.9% ethanol and sonicated for 0.6 h in order to remove completely the NIC molecules from the respective samples, then the solutions were syringe-filtered using a 450 nm porous PVDF membrane (Rejinold et al., 2021). This ultra-sonication and ethanol dissolution process effectively removes all NIC molecules from the precipitate. NIC concentration was measured in the solution by UV-Vis spectroscopy at 333 nm (Jasco-V630 Spectrophotometer, (Jasco Easton, Massachusetts, USA) (Yu et al., 2021). The NIC contents in NIC-X-LDH, ES100-NIC-X-LDH NPs, and the Tween 60-coated NPs were $\sim 28.14 \pm 2.56$, 20.93 ± 0.83 , and $14.02 \pm 1.29\%$, respectively.

In vitro Drug-release Study

The NIC release profile was tested based on an existing protocol (Pardhi et al., 2017) with a dissolution apparatus (DST-810 Lab Fine, Inc., Seoul, South Korea) under a constant temperature of 37°C, and a stirring frequency of ~ 50 rpm for 24 h. Drug release was conducted in two different solutions with pH values of 1.2 and 6.8, respectively, simulating a human's gastric and intestinal fluids (Otsuka et al., 2013), where 2% Tween 60 was dissolved in each solution. The ES100-NIC-X-LDH and Tween 60-ES100-NIC-X-LDH samples with identical NIC contents of 0.015 g were dispersed in a dissolution chamber. The aliquots were collected at pre-scheduled time intervals. For drug release, all the triplicated samples were evaluated by UV-Vis measurement at 333 nm.

Pharmacokinetic (PK) Study

Male Sprague-Dawley rats, ~ 0.3 kg in weight, were used for PK analysis as per previous protocols (Choi et al., 2021a; Yu et al., 2021), which were sanctioned by the Institutional Animal Care and Use Committee (IACUC No. IA21-00816) at Korea Conformity Laboratories (Incheon, Korea). Prior to the *in vivo* experiments, the rats were subjected to overnight fasting but with free access to water; thereafter, the dosage of 50 mg of NIC per kg was administered orally ($n = 5$) based on the formulation of Tween 60-ES100-NIC-X-LDH NPs. After oral administration, ~ 0.25 mL of blood sample was taken at pre-scheduled time intervals such as 0, 0.25, 0.5, 1, 2, 4, 6, 8, 12, and 24 h. Then the plasma was separated quickly by centrifugation at $43,456 \times g$ for 0.25 h at 4°C and kept at -70°C before analysis. Thereafter, the blood samples were

analyzed using a High-Performance Liquid Chromatography-Mass Spectrometry (HPLC-MS/MS) instrument (L2 SCIENCE Co., Ltd., Gyeonggi-do, Korea) to determine various PK parameters such as $t_{1/2}$ (elimination half-life), t_{\max} (time required to reach the C_{\max}), C_{\max} (maximum plasma concentration), and AUC (area under the plasma concentration–time curve).

Characterizations

The NMR spectra were measured with a Bruker/Magnet System 500'54 Ascend at Dankook University, Cheonan, South Korea, using D6-DMSO (Duetero.de, Sejong-si, 30128, South Korea) for all the experiments. The Fourier-transform infrared (FTIR) spectral studies were done using a Jasco FT-IR-6100 spectrometer (Jasco, Tokyo, Japan) using the standard KBr disk method in transmission mode (spectral range $4000\text{--}400\text{ cm}^{-1}$, resolution 1 cm^{-1} , 40 scans per spectrum). For FTIR, ~ 10 mg of each sample was mixed with 100 mg of KBr pellet; ground well using a mortar and pestle, and pelletized thereafter under a hydraulic press machine at 20 MPa for 1 min. The XRD pattern for each of the samples was measured with a Bruker D2 Phase diffractometer (Karlsruhe, Germany) equipped with $\text{CuK}\alpha$ radiation ($\lambda = 1.5418 \text{ \AA}$). All the data were recorded at the tube voltage and current of 30 kV and 10 mA, respectively. The step size was $\sim 0.02^\circ 2\theta$, and the scan range was $\sim 2\text{--}69.99^\circ 2\theta$. Dynamic Light Scattering (DLS) and zeta potential analyses were carried out using an Otsuka Electronics DLS/ZetaEL-SZ-2000 instrument (Otsuka, Japan) using disposable square cuvettes in both distilled water, and phosphate-buffered saline (PBS)gastro-intestinal solutions. The concentration of each sample for DLS and zeta potential was maintained at 10 mg/mL. UV-vis spectroscopy data were obtained using a Jasco-V630 Spectrophotometer (Easton, Massachusetts, USA), and the freeze-drying was carried out with an Ilshin Biobase instrument (Gyeonggi-do, South Korea) at -53°C . The field emission scanning electron microscopic (FE-SEM) analyses for various samples were done using a Sigma 300 (Carl Zeiss, Oberkochen, Germany) field-emission scanning electron microscope, using samples at a concentration of 1 mg/mL in distilled water and GIT solutions (pH 1.2 and 6.8). The samples prepared were dropped onto a silicon wafer using a 20 μL pipette and dried under ambient condition. For energy dispersive spectrometry (EDS) analyses, the samples were attached to the stub using double-sided carbon tape. All the samples were coated with platinum to reduce the electron charging effect. The elemental distributions of various samples such as recrystallized NIC, NIC-X-LDH NPs, ES100-NIC-X-LDH NPs, and Tween 60-NIC-X-LDH NPs were probed with FE-SEM and (EDS)-elemental mapping analyses (Carl Zeiss Sigma 300). Release studies were carried out using a temperature-controlled dissolution apparatus (DST-810 Lab Fine, Inc., Seoul, South Korea).

Statistical Analysis

The statistical significances of the differences were evaluated with a two-tailed Student's t-test. A P value of <0.05 was considered as statistically significant.

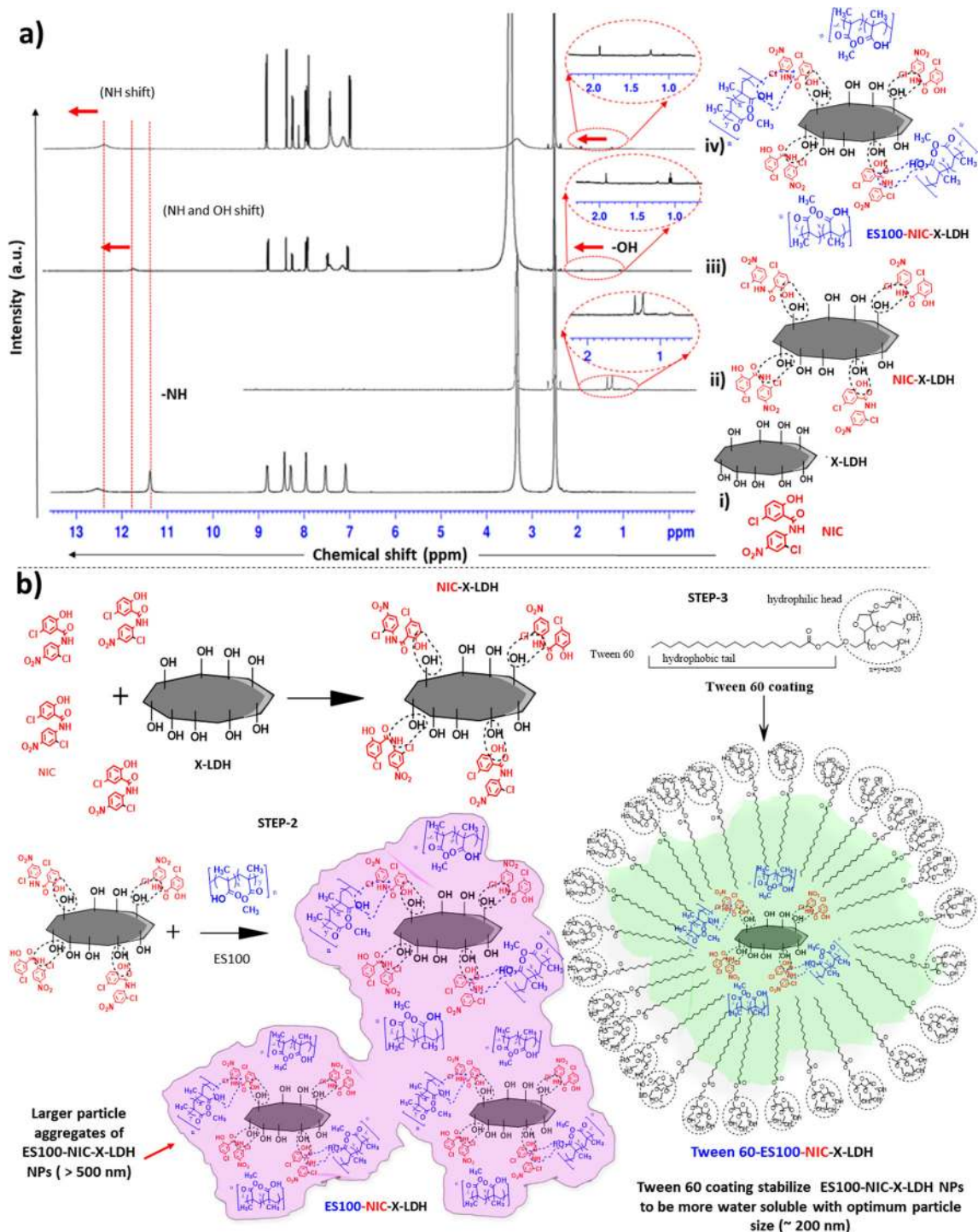


Fig. 3. Chemical interaction within ES100-NIC-X-LDH NPs: **a**) ^1H NMR spectroscopy evaluation of (i) control NIC; (ii) control X-LDH NPs, (iii) NIC-X-LDH NPs, and (iv) ES100-NIC-X-LDH NPs; **b**) structure model showing the predominant hydrogen-bonding interactions between X-LDH NPs and NIC, and ES100 molecules, whereas a hydrophobic–hydrophobic interaction is expected between Tween 60 and ES100-NIC-X-LDH NPs

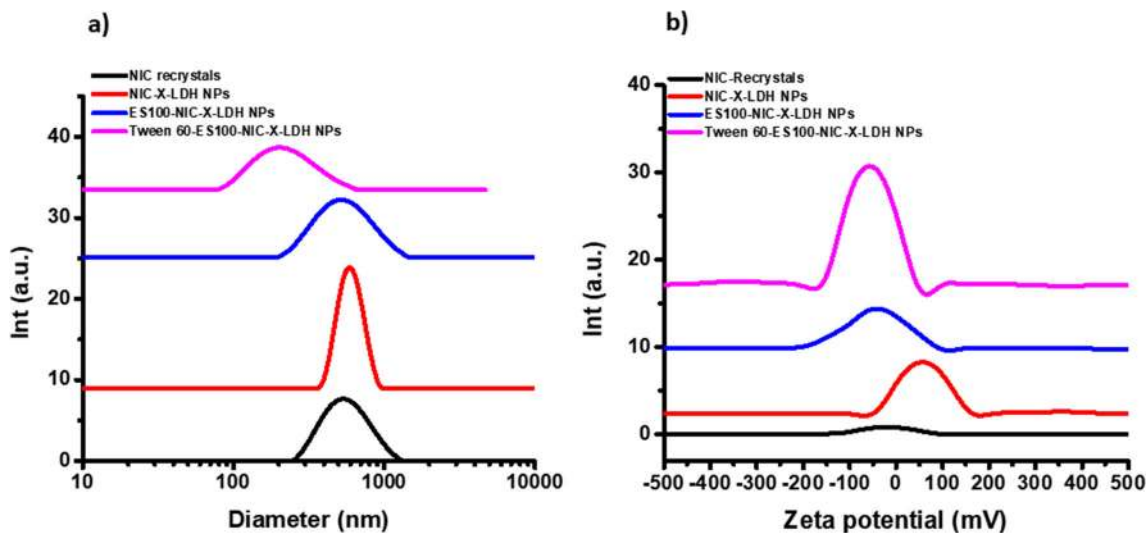


Fig. 4. **a** Particle-size analysis by DLS and **b** zeta potential measurement in distilled water (pH \approx 5.4) for the NIC recrystallized sample, NIC-X-LDH NPs, ES100-NIC-X-LDH NPs, and Tween 60-ES100-NIC-X-LDH NPs, respectively

RESULTS AND DISCUSSION

NMR and FTIR Characterizations

The possible interaction within Tween 60-ES100-NIC-X-LDH NPs was studied using FTIR analysis. Note that X-LDH and NIC could be interacting via hydrogen bonding predominantly through the amide proton of NIC with the hydroxyl groups on the X-LDH surface. In order to confirm this chemical interaction, an NMR analysis was done as shown in Fig. 3a. The characteristic amide proton in NIC was assigned to 11.4 ppm (Fig. 3a.i)(Jara et al., 2021), while the characteristic surface hydroxyl protons found in X-LDH were assigned to \sim 0.85 ppm and 1.2 ppm, respectively (Fig. 3a.ii)(Sideris et al., 2008). The amide proton in NIC and hydroxyl protons from X-LDH NPs were shifted downfield after interaction, indicating clearly their strong interaction via hydrogen bonding. Accordingly, the surface hydroxyl protons from X-LDH NPs were shifted downfield slightly to 1.2 ppm from 0.85 ppm, and to 1.9 ppm from 1.2 ppm, respectively, while the amide proton in the NIC molecule was also shifted downfield slightly to 11.8 ppm from 11.4 ppm with NIC-X-LDH NPs (Fig. 3a.iii), whereas the ES100-NIC-X-LDH NPs (Fig. 3a.iv) was also shifted strongly to 12.4 ppm. This characteristic downfield shift in the tested samples indicated clearly that strong hydrogen bonding interaction occurred not only between NIC and

X-LDH NPs, but also between ES100 and NIC-X-LDH NPs as indicated in the structure model (Fig. 3b).

The NMR analysis was further confirmed by the FTIR study as shown in Fig. S1 (Supplementary Material). The $-\text{NO}_2$ group in the NIC molecules could also induce a negative charge resulting in a strong interaction with the positively charged X-LDH NPs forming the NIC-X-LDH NPs. In addition, the characteristic C-Cl bond in NIC observed at between 800 and 400 cm^{-1} was shifted slightly after forming NIC-X-LDH NPs and subsequent modification with ES100 and Tween 60. Similarly, the band at $\sim 1518\text{ cm}^{-1}$, corresponding to the electronegative $-\text{NO}_2$ group in NIC, was shifted after bonding with X-LDH NPs and further coating with ES100 and Tween 60, indicating a contribution of charge interaction in addition to the hydrogen bonding for the formation of hybrid NPs (Fig. S1).

The disappearance of $-\text{NH}$ stretching at 3584 cm^{-1} and $-\text{OH}$ bending vibration at 1210 cm^{-1} in NIC-X-LDH NPs indicated a strong interaction between NIC and X-LDH NPs owing to the hydrogen bonding (Lodagekar et al., 2019) as confirmed by the NMR studies.

In the case of ES100-NIC-X-LDH NPs, the FTIR spectra showed a peak at 2953 cm^{-1} due to the presence of O-H (carboxylic acid), whereas the band at 1747 cm^{-1} owing to the C=O ester stretching was shifted slightly due to the hydroxyl interaction with the NIC molecules adsorbed on the X-LDH NPs. On the

Table 1. DLS and zeta potential measurements for various samples such as NIC recrystallized NPs, NIC-X-LDH NPs, ES100-NIC-X-LDH NPs, and Tween 60-ES100-NIC-X-LDH NPs, respectively

Samples	Size (nm)	PDI (a.u.)	Zeta potential (mV)
NIC recrystallized NPs	514.76 \pm 12.77	0.244 \pm 0.023	-15.90 ± 5.41
NIC-X-LDH NPs	710.16 \pm 17.11	0.304 \pm 0.016	53.79 \pm 4.53
ES100-NIC-X-LDH NPs	796.36 \pm 67.58	0.391 \pm 0.019	-39.99 ± 11.62
Tween 60-ES100-NIC-X-LDH NPs	215.56 \pm 08.72	0.358 \pm 0.024	-66.36 ± 13.63

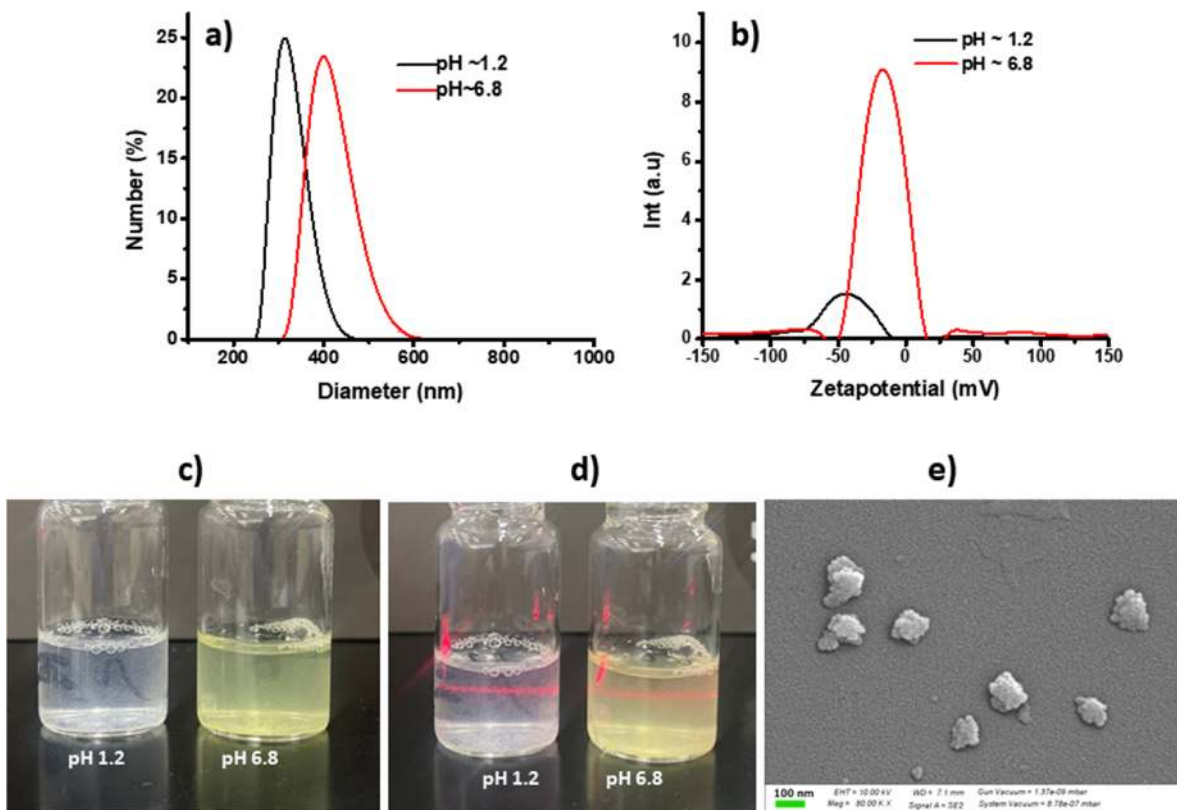


Fig. 5. **a** Particle-size analysis by DLS in solution at both pH 1.2 and 6.8 for the Tween 60-ES100-NIC-X-LDH NPs and **b** zeta potential analysis for the same; and **c** stable colloidal suspensions of Tween 60-ES100-NIC-X-LDH NPs at pH 1.2 and 6.8 and **d** Tyndall effects exhibited by their stable suspensions with pH 1.2 and 6.8; **e** FE-SEM for Tween 60-ES100-NIC-X-LDH NPs (Scalebar: 100 nm).

other hand, the peak at 1450 cm^{-1} corresponds to the CH_3 bending vibrations, whereas the C–O ester signal is found at 1153 cm^{-1} (Fig. S1a,b) (De Leo et al., 2020).

The Tween 60 coating on the final sample, ES100-NIC-X-LDH NP, was confirmed by observing the characteristic bands at 2925 and 2865 cm^{-1} , which are assigned for asymmetric (ν_s) and symmetric (ν_s) stretching bands for $-\text{CH}_2$ functional groups from the Tween 60. The band at 1729 cm^{-1} (C=O stretching in ester group) and the sharp peak at 3483 cm^{-1} (O–H stretching vibrations) further proved the physical coating on the sample (Fig. S1a). In addition, the improved solubility of Tween 60 coated samples indicated that the hydrophilic head groups of Tween 60 molecules might be projected outward while an inward hydrophobic–hydrophobic interaction might stabilize the coating of Tween 60 on the surface of ES100-NIC-X-LDH (Fig. 3b).

XRD, UV Spectroscopy, DLS and Zeta-potential Analysis

The pristine LDH NPs converted to single sheets, known as exfoliated LDH NPs (X-LDH) as shown in Fig. S2a. To understand this exfoliation process, XRD analysis was performed on pristine LDH as well as X-LDH NPs. According to the XRD analysis, pristine LDH NPs became X-ray amorphous upon exfoliation (Fig. S2b). On the other hand, both NIC-X-LDH NPs and ES100-NIC-X-LDH NPs showed recrystallized phases of NIC in aqueous solution (containing formamide and ethanol

solvents) (Fig. S3), indicating that NIC molecules were adsorbed successfully on the surface of the X-LDH NPs. In addition, the surface-adsorption process involved strong hydrogen bonding between hydroxyl groups of X-LDH NPs and amino/hydroxyl groups of NIC molecules as indicated by the NMR analysis (Fig. 3a). Similarly, the ES100 could bond on the surface of NIC-X-LDH NPs through a hydrogen bonding interaction. Both NIC-X-LDH NPs and ES100-NIC-X-LDH NPs showed characteristic peaks of a recrystallized NIC phase at $5.29, 10.8, 15.7, 20.03, 21.28, 23.47, 24.94, 25.77, 28.07, \text{ and } 30.26^\circ 2\theta$, confirming the possibility of recrystallization on the X-LDH surface. On the other hand, the Tween 60-coated sample showed an X-ray amorphous XRD pattern, indicating that the coating was successful and could enhance the solubility of NIC under in vitro and in vivo conditions. In reality, amorphous particles showed better solubility than their crystalline counterparts (Hancock & Parks, 2000). In the case of the Tween 60-coated sample, the amorphous nature could be due to the hydrophilic head group from Tween 60, oriented outward, as demonstrated in the structure model (Fig. 3b), making the final Tween 60-coated formulation very much water-soluble and dispersible compared to the un-coated one. Additional recrystallization experiments in various solvents and solutes were carried out in order to understand the recrystallization pattern of NIC, showing that the solvents rather than the solute predominantly affected NIC recrystallization (Figs S4, S5). Additional experiments will be performed later to understand more about the

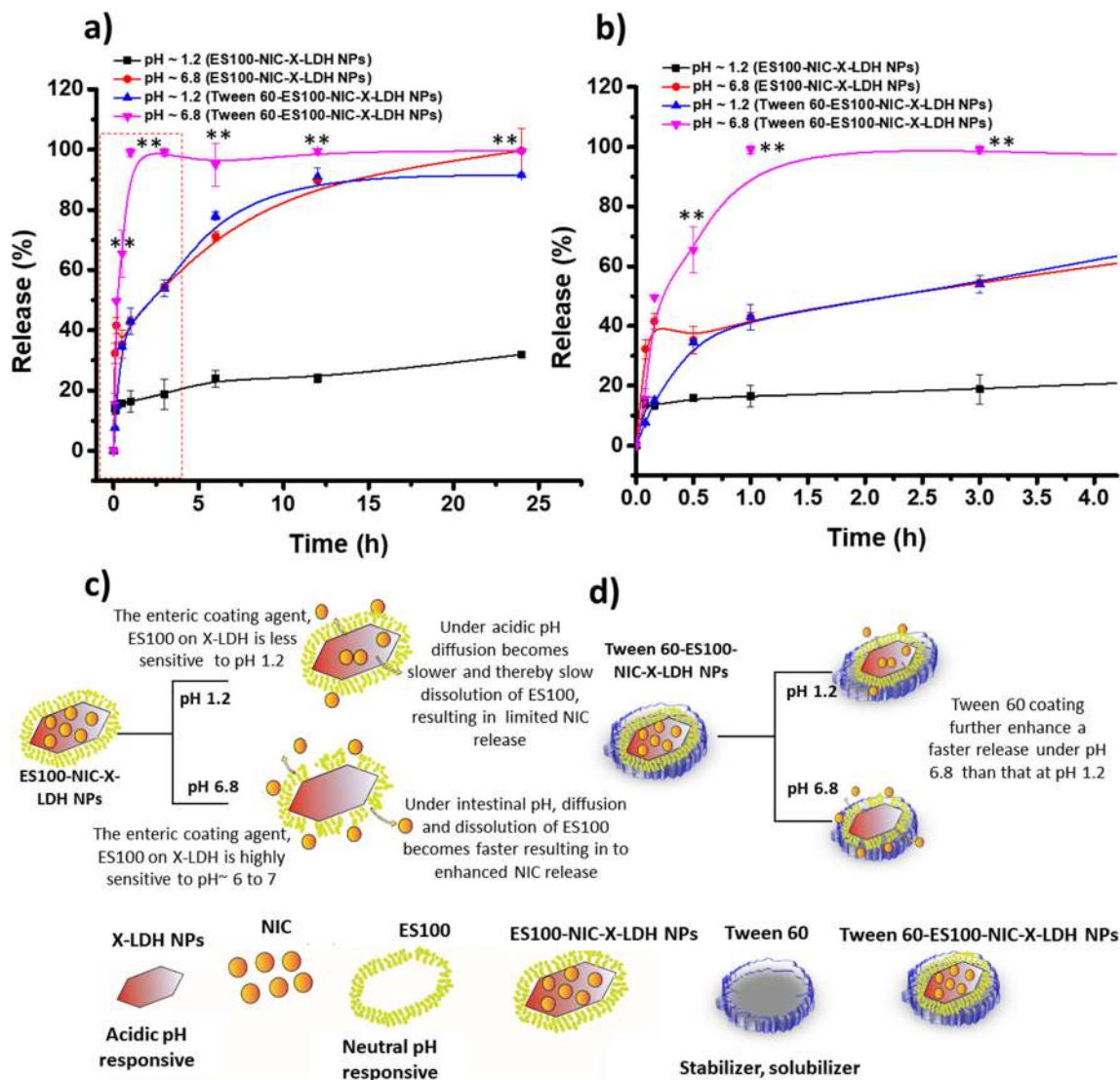


Fig. 6. pH-sensitive NIC release from **a**ES100-NIC-X-LDH NPs and Tween 60-ES100-NIC-X-LDH NPs at gastric solution pH (1.2) and intestinal solution pH (6.8) for 24 h and **b** the same during the initial 4 h; **c** a possible release mechanism via the pH-sensitive ES100-NIC-X-LDH NPs at pH 1.2 and 6; **d** Tween-60 coating further improves the stability of ES100-NIC-X-LDH NPs with enhanced NIC solubility, thereby leading to quicker release ($n = 3$, ** $p < 0.05$).

recrystallization characteristics of NIC under various solvent conditions.

To confirm the physical coating of Tween 60 on the samples, a UV-Vis spectroscopic analysis was also conducted which showed no specific red or blue shift, indicating that Tween 60 was coated on the external surface of the samples physically (Fig. S6). In addition, the particle-size analysis by DLS showed clearly that Tween 60 coating could increase the particle size from 350 to 520 nm in ethanol solvent (Fig. S7).

The DLS measurements for recrystallized NIC NPs, NIC-X-LDH NPs, ES100-NIC-X-LDH NPs, and Tween 60-ES100-NIC-X-LDH NPs were done in distilled water as shown in Fig. 4a. As expected, Tween 60-ES100-NIC-X-LDH NPs showed a stable particle size of $\sim 215.56 \pm 8.72$ nm whereas all other control samples had particle sizes

of >500 nm. This confirmed clearly the fact that better stability can be obtained with Tween 60 coating. In addition, the zeta potential analysis for the NIC-X-LDH NPs was determined to be $+53.79 \pm 4.53$ mV, which was changed to -66.36 ± 13.63 mV (Fig. 4b, Table 1) in the case of Tween 60-ES100-NIC-X-LDH NPs. Note that Tween 60 coating has dramatically improved the particle size and stability of NPs and might be beneficial for improved anti-viral efficacy in clinical perspectives. In addition, the NIC loaded in the X-LDH NPs could enable a clathrin-mediated endocytosis in the infected cell, thereby improving the therapeutic efficacy of the NIC hybrid drug significantly more than that of the intact NIC drug.

In addition, the particle size of Tween 60-ES100-NIC-X-LDH NPs was evaluated using DLS with gastrointestinal pH solutions. The particle size in a pH 6.8 solution was ~ 390 nm

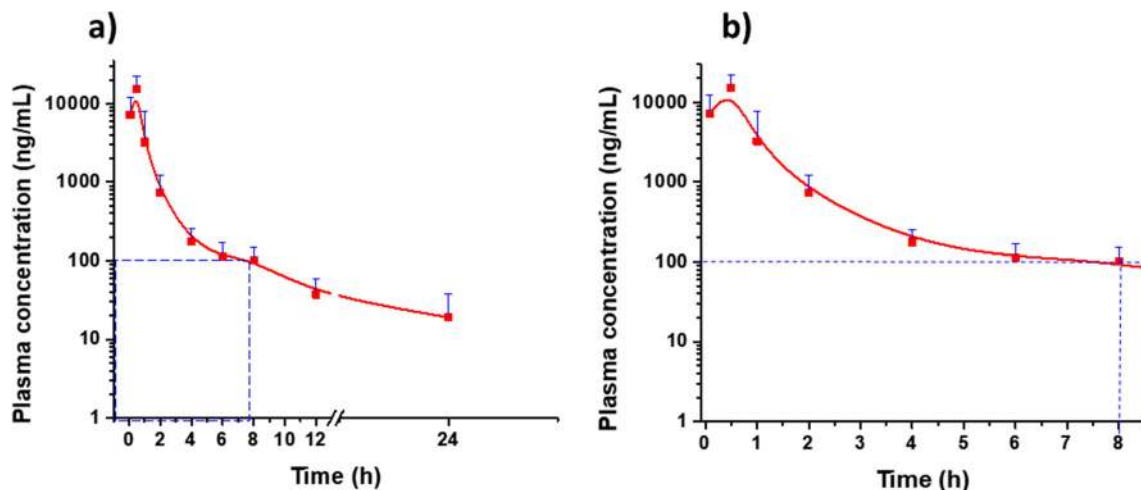


Fig. 7. The mean plasma concentration of NIC vs time after a single oral administration of Tween 60-ES100-NIC-X-LDH formulation in Sprague-Dawley rats; **a** up to 24 h and **b** initial 8 h results ($n = 5$, dosage 50 mg/kg NIC); the dotted lines in blue indicate the IC_{50} value for NIC against the SARS-CoV-2 virus

whereas it became 314 nm at pH 1.2 (Fig. 5a). According to the zeta potential analysis, the surface charge for Tween 60-ES100-NIC-X-LDH NPs at pH 1.2 was -44.97 ± 0.98 mV whereas at pH 6.8, it became -18 ± 2.82 mV (Fig. 5b). The samples at gastrointestinal pH solution remained as a stable suspension as shown in Fig. 5c with a very good Tyndall effect (Li et al., 2018)(Fig. 5d).

FE-SEM and Elemental Mapping

As shown in Fig. 5e, the FE-SEM image for Tween 60-ES100-NIC-X-LDH NPs showed the particle size to be ~ 200 nm. On the other hand, the morphology of samples such as NIC, NIC-X-LDH NPs, and ES100-NIC-X-LDH NPs under the same solvent conditions of ethanol/formamide/distilled water showed a featureless morphology but a kind of aggregated form of particles with sizes of ~ 500 , ~ 700 , and ~ 800 nm, respectively (Fig. S8a–c). On the contrary, the Tween 60-ES100-NIC-X-LDH NPs had a spherical morphology (Fig. 5e) having a smaller particle size with good stability in an aqueous solution (Fig. S6b, c), indicating that the NIC drug

molecules were loaded successfully on the X-LDH NPs. As the particle size was in the optimum range of <200 nm, this formulation should be beneficial for effectively targeting the SARS-CoV-2 virus through an extracellular/intracellular pathway (Vonnemann et al., 2014). NIC has been known to exert anti-viral properties by inhibiting endocytosis, autophagy, and replication, thereby preventing further maturation of viral particles within the infected cells (Pindiprolu & Pindiprolu, 2020).

The elemental mapping analysis also confirmed the presence of all the components such as X-LDH NPs and NIC in the composite particles of Tween 60-ES100-NIC-X-LDH NPs (Fig. S9).

In vitro NIC Release Studies

The release studies were conducted at pH 1.2 and 6.8, mimicking the gastric (Evans et al., 1988) and intestinal conditions, respectively (Koziolek et al., 2015). A significantly greater NIC release from ES100-NIC-X-LDH was observed (Fig. 6a,b) under the intestinal pH condition, and reached $\sim 100\%$ in 24 h, whereas a restricted release of $\sim 30\%$ was observed at pH 1.2 for the same time period. In order to understand the effect of Tween 60 coating on the NIC release, release studies were done using Tween 60-ES100-NIC-X-LDH NPs under pH conditions of 1.2 and 6.8, both having 2% Tween 60 in the dissolution media. At pH 6.8, $\sim 100\%$ of the drug was released in only 1 h at pH 6.8 (Fig. 6a,b), much faster and more completely than under pH 1.2 conditions. Compared to the uncoated sample, coating with Tween 60 increased both the extent and rate of release at both pH values, indicating that coating should be beneficial for enhanced NIC release, especially in the intestinal site.

The enhanced release of NIC at intestinal pH could be due mainly to the improved stability and solubility of NIC when it was composited with ES100 and Tween 60 along with X-LDH NPs. In addition, ES100 can enhance colon-specific targeting (Hales et al., 2020; Rehman et al., 2020), which would also be beneficial for COVID-19 patients because the viral loads in the

Table 2. PK parameters for NIC from Tween 60-ES100-NIC-X-LDH oral formulation after a single oral administration (50 mg/kg) in rats ($n=5$)

PK parameters	
* $t_{1/2}$ (h)	4.86 ± 0.84
** t_{max} (h)	0.60 ± 0.22
** C_{max} (ng/mL)	15328.82 ± 6854.44
*** AUC_{last} (ng·h/mL)	13924.76 ± 4087.19
*** $AUC_{infinite}$ (ng·h/mL)	14060.05 ± 4197.42

* $t_{1/2}$ = elimination half-life

** t_{max} = time required to reach the C_{max}

*** C_{max} = maximum plasma concentration

*** AUC = area under the plasma concentration–time curve

Table 3. PK parameters reported for NIC with various oral formulations

Previous NIC formulations	characteristics	C_{max} (ng/mL)	t_{max} (h)	AUC (ng·h/mL)	Remarks	Application	Ref
NIC-HP- β -CD inclusion complex	Physical complex	1277.93 \pm 221	0.28 \pm 0.12	3475	Oral administration (50 mg/kg) in Balb/c mouse	<i>In-vitro</i> anti-cancer therapy	(Lodagekar et al., 2019)
Solid Lipid NPs	200 nm size	3947 \pm 240	12 \pm 0.1	16740	Oral administration (100 mg/kg) in rabbits	Improved PK for NIC	(Rehman et al., 2018)
NIC-CSLEs	307 nm	432 \pm 21	3	2457	Oral administration (20 mg/kg) in rats	PK studies of NIC formulation	(Zhang et al., 2015)
NIC-PSLEs	162 nm	726 \pm 40	0.3	2582	Oral administration (20 mg/kg) in rats	PK studies of NIC formulation	(Zhang et al., 2015)
Tween 60-ES100-NIC-X-LDH NPs	~200 nm size (as per the FE-SEM)	15328.82 \pm 6854.44	0.6	14060	Oral administration (50 mg/kg) in rats	Towards SARS-CoV-2 infections	Present study

GI tract were reported to be significantly greater than for other organs. As demonstrated schematically in Fig. 6c, the release mechanism for NIC from ES100-NIC-X-LDH NPs could be rationalized mainly by the combined action of ES100 and Tween 60. The latter contributed mainly to the dissolution of the oral drug present regardless of the pH conditions but the former played a decisive role in the drug release under a gastrointestinal solution condition; the NIC release was fairly restricted under an acidic condition due to the low solubility of ES100 at pH 1.2, whereas the 100% release at pH 6.8 was observed because of the swelling and the dissolution of ES100 providing the diffusion pathways of NIC molecules out of ES100-NIC-X-LDH NPs. Here, one of the research goals was to induce a controlled release in the target intestinal site (Khan et al., 2000); therefore, the as-made oral formulation with pH responsive molecules such as ES100 and X-LDH NPs could help to improve the controlled NIC release in vivo. To understand the release kinetics mechanism, the release parameters were fitted to different kinetic equations such as zero-order, first-order, Higuchi Model, Hixon-Crowell Model, and Korsmeyer-Peppas Model (Figs S10, S11). The maximum r^2 value of 0.9707 was obtained for the Higuchi model and of 0.9877 for the Korsmeyer-Peppas model for the ES100-NIC-X-LDH NPs (Table S1), when the NIC-release experiments were performed at pH 6.8. A similar trend was shown by the Tween 60-ES100-NIC-X-LDH NPs. Such results are in good agreement with the hypothesis shown in Fig. 6c, because they have been applied generally to the swelling, dissolution, and degradation mechanisms. On the other hand, as expected, the zero- and first-order kinetic equations did not fit the NIC release from hybrid NPs.

In vivo PK Analysis

PK analysis was conducted for Tween 60-ES100-NIC-X-LDH NPs (50 mg/kg) after a single oral administration in rats. The main reason for choosing only Tween 60-ES100-NIC-X-LDH NPs was due to its better stability, optimum particle size, and enhanced drug release (Fig. 6) compared to the uncoated sample. As shown in Fig. 7a,b, the plasma NIC concentration from Tween 60-ES100-NIC-X-LDH NPs maintained its IC₅₀ value at least up to 8 h. In order to have a clear understanding of the quantitative data, various PK parameters such as $t_{1/2}$, C_{max} , t_{max} , and AUC were also calculated (Table 2).

Tween 60-ES100-NIC-X-LDH NPs showed a very high AUC_{last} value of 13924.76 \pm 4087.19 ng·h/mL with a $t_{1/2}$ of 4.86 \pm 0.84 h. In addition, the value for C_{max} was significantly higher at 15328.82 \pm 6854.44 ng/mL with a t_{max} of 0.60 \pm 0.22 h. The prolonged elimination half-life of NIC in the plasma from Tween 60-ES100-NIC-X-LDH NPs could be attributed to sustained NIC release capability as demonstrated in the in vitro release studies (Fig. 6a,b). Note that even with a very low dosage of 50 mg/kg, Tween 60-ES100-NIC-X-LDH NPs were able to retain the therapeutic concentration for longer than intact NIC, indicating its possible benefits for treating COVID-19 patients. The present formulation showed very high PK parameters, C_{max} (~15,000 ng/mL), t_{max} (0.60 h), and AUC (~14,000 ng·h/mL), compared to those of commercially

available Yomesan® , which had C_{\max} (~155 ng/mL), t_{\max} (4 h), and AUC (~1100 ng·h/mL), according to the previous study (Yu et al., 2021).

CLINICAL PERSPECTIVES

COVID-19 has caused a surging, highly contagious, multi-variant pandemic; the scientific community has responded in many ways, using its knowledge and skills. Tremendous improvements have been made in terms of detection, diagnosis, and therapeutic strategy using nanomaterials. Disadvantages associated with each technique make the scaling up of such lab solutions to factory-scale products difficult, especially as quickly as expected or needed. On the other hand, though various vaccination strategies are emerging, both in developing and developed countries, their actual effectiveness for long-term immunity is still unknown. Nanomaterials are needed for effective delivery of existing potential antiviral drugs such as NIC, which has been repurposed for a wide variety of pathological conditions such as cancers, bacterial and viral infections, etc. Interestingly, Tween 60-ES100-NIC-X-LDH NPs allowed very high NIC concentration (C_{\max}) in the plasma after 30 min with a maximum concentration of ~15,000 ng/mL, which is the highest value among the data reported in Table 3.

The present authors believe that the oral formulation discussed here, ES100-NIC-X-LDH NPs, would be useful in the fight against SARS-CoV-2 viral infections with no significant harmful effects to the human body, as the individual components comprising ES100-NIC-X-LDH NPs are biocompatible and biodegradable.

CONCLUSIONS

The oral formulation based on Tween 60-ES100-NIC-X-LDH NPs was developed successfully for NIC delivery against COVID-19, and was further characterized using NMR, FTIR, FESEM, and EDS to check its physicochemical properties. In vitro NIC release was determined to be significantly greater at the pH (6.8) of intestinal solutions compared to that (1.2) of gastric solutions, confirming that the dissolution property of NIC was greatly improved at pH 6.8, thanks to the enteric coating effect of ES100 and stabilization by Tween 60. In the present PK study, the highest plasma concentration of NIC was obtained after a single oral administration, maintaining the required IC_{50} value for up to 8 h with a low dose of 50 mg/kg. In addition to the improved C_{\max} value, the AUC was also greatly enhanced compared to those values obtained from previous oral formulations. The present repurposed NIC hybrid drug, Tween 60-ES100-NIC-X-LDH NPs, could, therefore, be a potential anti-viral technology for tackling SARS-CoV-2 infections.

SUPPLEMENTARY INFORMATION

The online version contains supplementary material available at <https://doi.org/10.1007/s42860-021-00153-6>.

ACKNOWLEDGMENTS

This research was supported by Basic Science Research Program through the National Research Foundation of Korea (NRF) funded by the Ministry of Education (No. 2020R111A2074844), by the NRF grant funded by the Korea government (MSIT) (No. 2020R1F1A1075509), and under the framework of the International Cooperation Program managed by NRF (No. 2017K2A9A2A10013104).

FUNDING

Funding sources are as stated in the Acknowledgments.

Declarations

Conflict of Interest

The authors declare that they have no conflict of interest.

REFERENCES

- Ansy, K. M., Lee, J.-H., Piao, H., Choi, G., & Choy, J.-H. (2018). Stabilization of antioxidant gallate in layered double hydroxide by exfoliation and reassembling reaction. *Solid State Sciences*, 80, 65–71. <https://doi.org/10.1016/j.solidstatesciences.2018.04.001>
- Belgheisi, G., Nazarpak, M. H., & Hashjin, M. S. (2020). Bone tissue engineering electrospun scaffolds based on layered double hydroxides with the ability to release vitamin D3: Fabrication, characterization and in vitro study. *Applied Clay Science*, 185, 105434. <https://doi.org/10.1016/j.clay.2019.105434>
- Choi, G., & Choy, J.-H. (2021). Recent progress in layered double hydroxides as a cancer theranostic nanoplat form. *WIREs Nanomedicine and Nanobiotechnology*, 13(2), e1679. <https://doi.org/10.1002/wnan.1679>
- Choi, G., Jeon, I.-R., Piao, H., & Choy, J.-H. (2018a). Highly condensed boron cage cluster anions in 2d carrier and its enhanced antitumor efficiency for boron neutron capture therapy. *Advanced Functional Materials*, 28(27), 1704470. <https://doi.org/10.1002/adfm.201704470>
- Choi, G., Kim, T.-H., Oh, J.-M., & Choy, J.-H. (2018b). Emerging nanomaterials with advanced drug delivery functions; focused on methotrexate delivery. *Coordination Chemistry Reviews*, 359, 32–51. <https://doi.org/10.1016/j.ccr.2018.01.007>
- Choi, G., Piao, H., Rejinold, N. S., Yu, S., Kim, K.-Y., Jin, G.-W., & Choy, J.-H. (2021a). Hydrotalcite–niclosamide nanohybrid as oral formulation towards SARS-CoV-2 viral infections. *Pharmaceuticals*, 14(5). <https://doi.org/10.3390/ph14050486>
- Choi, G., Rejinold, N. S., Piao, H., & Choy, J.-H. (2021b). Inorganic–inorganic nanohybrids for drug delivery, imaging and photo-therapy: recent developments and future scope. *Chemical Science*, 12(14), 5044–5063. <https://doi.org/10.1039/D0SC06724E>
- De Leo, V., Di Gioia, S., Milano, F., Fini, P., Comparelli, R., Mancini, E., Agostiano, A., Conese, M., & Catucci, L. (2020). Eudragit S100 entrapped liposome for curcumin delivery: anti-oxidative effect in Caco-2 cells. *Coatings*, 10(2). <https://doi.org/10.3390/coatings10020114>
- Evans, D. F., Pye, G., Bramley, R., Clark, A. G., Dyson, T. J., & Hardcastle, J. D. (1988). Measurement of gastrointestinal pH profiles in normal ambulant human subjects. *Gut*, 29(8), 1035. <https://doi.org/10.1136/gut.29.8.1035>
- Grifasi, F., Chierotti, M. R., Gaglioti, K., Gobetto, R., Maini, L., Braga, D., Dichiarante, E., & Curzi, M. (2015). Using salt cocrystals to improve the solubility of niclosamide. *Crystal Growth & Design*, 15(4), 1939–1948. <https://doi.org/10.1021/acs.cgd.5b00106>

- Hales, D., Tefas, L. R., Tomuta, I., Moldovan, C., Gulei, D., Munteanu, R., & Porfire, A. (2020). Development of a curcumin-loaded polymeric microparticulate oral drug delivery system for colon targeting by quality-by-design approach. *Pharmaceutics*, *12*(11), 1027. <https://doi.org/10.3390/pharmaceutics12111027>
- Hancock, B. C., & Parks, M. (2000). What is the true solubility advantage for amorphous pharmaceuticals? *Pharmaceutical Research*, *17*(4), 397–404. <https://doi.org/10.1023/A:1007516718048>
- Hatamipour, M., Jaafari, M. R., Momtazi-Borojeni, A. A., Ramezani, M., & Sahebkar, A. (2019). Nanoliposomal encapsulation enhances in vivo anti-tumor activity of niclosamide against melanoma. *Anticancer Agents in Medicinal Chemistry*, *19*(13), 1618–1626. <https://doi.org/10.2174/1871520619666190705120011>
- Hu, J., Li, C., Wang, S., Li, T., & Zhang, H. (2020). Genetic variants are identified to increase risk of COVID-19 related mortality from UK Biobank data. *medRxiv*. <https://doi.org/10.1101/2020.11.05.20226761>
- Huang, M., Qiu, Q., Zeng, S., Xiao, Y., Shi, M., Zou, Y., Ye, Y., Liang, L., Yang, X., & Xu, H. (2015). Niclosamide inhibits the inflammatory and angiogenic activation of human umbilical vein endothelial cells. *Inflammation Research*, *64*(12), 1023–1032. <https://doi.org/10.1007/s00011-015-0888-8>
- Jara, M. O., Warnken, Z. N., & Williams 3rd., R. O. (2021). Amorphous solid dispersions and the contribution of nanoparticles to in vitro dissolution and in vivo testing: niclosamide as a Case Study. *Pharmaceutics*, *13*(1). <https://doi.org/10.3390/pharmaceutics13010097>
- Jeon, S., Ko, M., Lee, J., Choi, I., Byun, S. Y., Park, S., Shum, D., & Kim, S. (2020). Identification of antiviral drug candidates against SARS-CoV-2 from FDA-approved drugs. *Antimicrobial Agents and Chemotherapy*, *64*(7), e00819–e00820. <https://doi.org/10.1128/AAC.00819-20>
- Jin, W., & Park, D.-H. (2019). Functional Layered Double Hydroxide Nanohybrids for Biomedical Imaging. *Nanomaterials (Basel, Switzerland)*, *9*(10), 1404. <https://doi.org/10.3390/nano9101404>
- Kao, J. C., HuangFu, W. C., Tsai, T. T., Ho, M. R., Jhan, M. K., Shen, T. J., Tseng, P. C., Wang, Y. T., & Lin, C. F. (2018). The antiparasitic drug niclosamide inhibits dengue virus infection by interfering with endosomal acidification independent of mTOR. *PLoS Neglected Tropical Diseases*, *12*(8), e0006715. <https://doi.org/10.1371/journal.pntd.0006715>
- Khan, M. Z. I., Stedul, H. P., & Kurjakovic, N. (2000). A pH-dependent colon-targeted oral drug delivery system using methacrylic acid copolymers. II. Manipulation of drug release using Eudragit (R) L100 and Eudragit S100 combinations. *Drug Development and Industrial Pharmacy*, *26*(5), 549–554. <https://doi.org/10.1081/Ddc-100101266>
- Koziolek, M., Grimm, M., Becker, D., Jordanov, V., Zou, H., Shimizu, J., Wanke, C., Garbacz, G., & Weitschies, W. (2015). Investigation of pH and temperature profiles in the gi tract of fasted human subjects using the intellicap® system. *Journal of Pharmaceutical Sciences*, *104*(9), 2855–2863. <https://doi.org/10.1002/jps.24274>
- Li, S., Rui, L., Bekana, D., & Lai, Y. (2018). Self-assembly of supramolecular nanotubes/microtubes from 3,5-Dimethyl-4-iodopyrazole for plasmonic nanoparticle organization. *Nanoscale*, *10*. <https://doi.org/10.1039/C8NR07372D>
- Li, M., Guo, X., & Wang, X. (2021). Retrospective prediction of the epidemic trend of COVID-19 in Wuhan at four phases. *Journal of Medical Virology*. <https://doi.org/10.1002/jmv.26781>
- Lodagekar, A., Borkar, R. M., Thatikonda, S., Chavan, R. B., Naidu, V. G. M., Shastri, N. R., Srinivas, R., & Chella, N. (2019). Formulation and evaluation of cyclodextrin complexes for improved anticancer activity of repurposed drug: Niclosamide. *Carbohydrate Polymers*, *212*, 252–259. <https://doi.org/10.1016/j.carbpol.2019.02.041>
- Ma, R., Liu, Z., Li, L., Iyi, N., & Sasaki, T. (2006). Exfoliating layered double hydroxides in formamide: a method to obtain positively charged nanosheets. *Journal of Materials Chemistry*, *16*(39), 3809–3813. <https://doi.org/10.1039/B605422F>
- Ma, R., Ma, Z. G., Gao, J. L., Tai, Y., Li, L. J., Zhu, H. B., Li, L., Dong, D. L., & Sun, Z. J. (2020). Injectable pegylated niclosamide (polyethylene glycol-modified niclosamide) for cancer therapy. *Journal of Biomedical Materials Research A*, *108*(1), 30–38. <https://doi.org/10.1002/jbm.a.36788>
- Mei, Q., Wang, F., Bryant, A., Wei, L., Yuan, X., & Li, J. (2021). Mental health problems among COVID-19 survivors in Wuhan, China. *World Psychiatry*, *20*(1), 139–140. <https://doi.org/10.1002/wps.20829>
- Otsuka, K., Shono, Y., & Dressman, J. (2013). Coupling biorelevant dissolution methods with physiologically based pharmacokinetic modelling to forecast in-vivo performance of solid oral dosage forms. *Journal of Pharmacy and Pharmacology*, *65*, 937–952. <https://doi.org/10.1111/jphp.12059>
- Pardhi, V., Chavan, R. B., Thipparaboina, R., Thatikonda, S., Naidu, V. G. M., & Shastri, N. R. (2017). Preparation, characterization, and cytotoxicity studies of niclosamide loaded mesoporous drug delivery systems. *International Journal of Pharmaceutics*, *528*(1), 202–214. <https://doi.org/10.1016/j.ijpharm.2017.06.007>
- Pindiprolu, S. K. S. S., & Pindiprolu, S. H. (2020). Plausible mechanisms of Niclosamide as an antiviral agent against COVID-19. *Medical Hypotheses*, *140*, 109765–109765. <https://doi.org/10.1016/j.mehy.2020.109765>
- Rehman, M. U., Khan, M. A., Khan, W. S., Shafique, M., & Khan, M. (2018). Fabrication of Niclosamide loaded solid lipid nanoparticles: in vitro characterization and comparative in vivo evaluation. *Artificial Cells, Nanomedicine, and Biotechnology*, *46*(8), 1926–1934. <https://doi.org/10.1080/21691401.2017.1396996>
- Rehman, S., Ranjha, N. M., Raza, M. R., Hanif, M., Majed, A., & Ameer, N. (2020). Enteric-coated Ca-alginate hydrogel beads: a promising tool for colon targeted drug delivery system. *Polymer Bulletin*. <https://doi.org/10.1007/s00289-020-03359-1>
- Rejinold, N. S., Choi, G., Piao, H., & Choy, J.-H. (2021). Bovine Serum Albumin-Coated Niclosamide-Zein Nanoparticles as Potential Injectable Medicine against COVID-19. *Materials*, *14*(14). <https://doi.org/10.3390/ma14143792>
- Sideris, P. J., Nielsen, U. G., Gan, Z., & Grey, C. P. (2008). Mg/Al ordering in layered double hydroxides revealed by multinuclear NMR spectroscopy. *Science*, *321*(5885), 113. <https://doi.org/10.1126/science.1157581>
- Vonnemann, J., Sieben, C., Wolff, C., Ludwig, K., Böttcher, C., Herrmann, A., & Haag, R. (2014). Virus inhibition induced by polyvalent nanoparticles of different sizes. *Nanoscale*, *6*(4), 2353–2360. <https://doi.org/10.1039/C3NR04449A>
- Yamamoto, V., Bolanos, J. F., Fiallos, J., Strand, S. E., Morris, K., Shahrokhinia, S., Cushing, T. R., Hopp, L., Tiwari, A., Hariri, R., Sokolov, R., Wheeler, C., Kaushik, A., Elsayegh, A., Eliashiv, D., Hedrick, R., Jafari, B., Johnson, J. P., Khorsandi, M., et al. (2020). COVID-19: Review of a 21st century pandemic from etiology to neuro-psychiatric implications. *Journal of Alzheimer's Disease*, *77*, 459–504. <https://doi.org/10.3233/JAD-200831>
- Yan, L., Gonca, S., Zhu, G., Zhang, W., & Chen, X. (2019). Layered double hydroxide nanostructures and nanocomposites for biomedical applications. *Journal of Materials Chemistry B*, *7*(37), 5583–5601. <https://doi.org/10.1039/c9tb01312a>
- Yang, Y. T., Xing, X., Sreekissoon, S., & Li, Z. (2021). Impact of transmission control measures on the epidemiology of maxillofacial injuries in Wuhan City during the COVID-19 epidemic. *Journal of Craniofacial Surgery*. Publish Ahead of Print. <https://doi.org/10.1097/SCS.00000000000007427>
- Yu, X., Liu, F., Zeng, L., He, F., Zhang, R., Yan, S., Zeng, Z., Shu, Y., Zhao, C., Wu, X., Lei, J., Zhang, W., Yang, C., Wu, K., Wu, Y., An, L., Huang, S., Ji, X., Gong, C., et al. (2018). Niclosamide Exhibits Potent Anticancer Activity and Synergizes with Sorafenib in Human Renal Cell Cancer Cells. *Cellular Physiology and Biochemistry*, *47*(3), 957–971. <https://doi.org/10.1159/000490140>
- Yu, S., Piao, H., Rejinold, N. S., Jin, G., Choi, G., & Choy, J.-H. (2021). Niclosamide-Clay Intercalate Coated with Nonionic Polymer for Enhanced Bioavailability toward COVID-19

- Treatment. *Polymers*, 13(7). <https://doi.org/10.3390/polym13071044>
- Zhang, X., Zhang, Y., Zhang, T., Zhang, J., & Wu, B. (2015). Significantly enhanced bioavailability of niclosamide through sub-micron lipid emulsions with or without PEG-lipid: a comparative study. *Journal of Microencapsulation*, 32(5), 496–502. <https://doi.org/10.3109/02652048.2015.1057251>
- Zhu, G., Zhu, Y., Wang, Z., Meng, W., Wang, X., Feng, J., Li, J., Xiao, Y., Shi, F., & Wang, S. (2021). The association between ambient temperature and mortality of the coronavirus disease 2019 (COVID-19) in Wuhan, China: a time-series analysis. *BMC Public Health*, 21(1), 117. <https://doi.org/10.1186/s12889-020-10131-7>

(Received 2 May 2021; revised 12 August 2021; AE: L. Williams)